

$\Sigma 3(111)$ grain boundary of body-centered cubic Ti-Mo and Ti-V alloys: First-principles and model calculations

Jia-Yi Yan,^{*} Hossein Ehteshami, Pavel A. Korzhavyi, and Annika Borgenstam

Department of Materials Science and Engineering, KTH Royal Institute of Technology, Brinellvägen 23, 100 44 Stockholm, Sweden

(Received 2 April 2017; published 5 July 2017)

The energetics and atomic structures of $\Sigma 3[1\bar{1}0](111)$ grain boundary (GB) of body-centered cubic (bcc) Ti-Mo and Ti-V alloys are investigated using density-functional-theory calculations and virtual crystal approximation. The electron density in bcc structure and the atomic displacements and excess energy of the GB are correlated to bcc- ω phase stability. Model calculations based on pairwise interplanar interactions successfully reproduce the chemical part of GB energy. The chemical GB energy can be expressed as a sum of excess pairwise interactions between bcc (111) layers, which are obtained from Gaussian elimination of the total energies of a number of periodic structures. The energy associated with the relaxation near the GB is solved by numerical minimization using the derivatives of the excess interactions. Anharmonic interlayer interactions are necessary for obtaining accurate relaxation energy and excess GB volume from model calculations. The effect of GB on vibrational spectrum is also investigated. Segregation energies of B and Y to a substitutional site on the GB plane are calculated. Preliminary results suggest that Y tends to segregate, while B tends to antisegregate.

DOI: [10.1103/PhysRevMaterials.1.023602](https://doi.org/10.1103/PhysRevMaterials.1.023602)

I. INTRODUCTION

Body-centered cubic (bcc) Ti is thermodynamically stable above 1155 K under ambient pressure. Upon cooling, it transforms to hexagonal close-packed (hcp) Ti, which is stable down to room temperature [1]. Pure bcc-Ti is mechanically unstable at 0 K under ambient pressure, featured by a negative C' shear modulus and imaginary phonon frequencies [2]. Therefore, it is not possible to investigate bcc grain boundary (GB) structures using first-principles total energy calculations at 0 K, because any disturbance caused by GB will lead to a collapse of bcc structure.

To stabilize bcc Ti using first-principles methods, one has to explicitly include atomic vibrations corresponding to a temperature where bcc Ti is stable, for instance, using molecular dynamics and assigning proper displacements and velocities to the atoms. In recent years, several methods have emerged for bcc Ti and other phases mechanically unstable at 0 K [3–6]. However, applying these methods directly to a supercell containing GBs, which is probably hundreds or thousands of times more expensive, is still a formidable task for today's computational power. It is therefore desirable to extract information from crystal structures related to a GB yet much smaller than a GB supercell. Using such information, the energetics and structures of a GB can be obtained from model calculations.

Another route to approach the mechanically unstable bcc Ti is by changing the chemical composition. By alloying Ti with elements like V and Mo, the bcc-to-hcp transformation temperature can be brought down to 0 K, stabilizing bcc structure with respect to hcp and another structure, ω phase [1]. This enables meaningful total-energy calculations of bcc GBs. By adjusting the chemical compositions, one can obtain a series of phase stabilities and GB properties, which helps reveal the correlations between them.

In this paper, we calculate bcc GB energy from a supercell and also explore the feasibility of extracting GB properties from smaller structures that are lighter to calculate. We first benchmark virtual crystal approximation (VCA) [7] for Ti-Mo and Ti-V alloys. Second, we present first-principles calculations of GB supercells using VCA, from which GB energies and atomic structures are obtained. Finally, analytical models are constructed for a number of static and dynamic GB properties of interest.

We have also calculated the segregation energies of B and Y to a substitutional site on the GB plane. The results are regarded as preliminary, as described in Appendix A.

II. FIRST-PRINCIPLES CALCULATIONS

A. Methodology

We have carried out 0 K frozen-ion density-functional-theory (DFT) calculations using Quantum Espresso (QE) [8]. The ultrasoft pseudopotentials (USPP) of Ti, Mo, and V are taken from the Garrity–Bennett–Rabe–Vanderbilt library [9], where the exchange-correlation energy takes the general gradient approximation (GGA) by Perdew, Burke, and Ernzerhof [10]. Virtual crystal approximation (VCA) [7] is adopted and the USPPs of Ti-Mo and Ti-V alloys are prepared by mixing the USPPs of the pure elements. We use a wave-function energy cutoff of 40 Ry (1 Ry = 13.6057 eV), an electron-density cutoff energy of 480 Ry, and a first-order Methfessel–Paxton smearing [11] with a width of 0.005 Ry. A Monkhorst–Pack k -point mesh [12] of $24 \times 24 \times 24$ is used for a bcc unit cell, and $4 \times 8 \times 14$ for the GB supercell described below. Equilibrium bcc lattice parameter for each Ti-Mo and Ti-V alloy is found, and the second-order elastic constants C_{11} , C_{12} , and C_{44} are calculated by tetragonal and orthorhombic distortions [13]. Phonon frequencies are calculated by density-functional perturbation theory [14] using QE. The 0 K total energies of hcp and ω phases are also calculated using the same settings except the k mesh ($22 \times 22 \times 14$ for hcp and $14 \times 14 \times 19$ for ω primitive cells).

^{*}jiaiyiyan@kth.se

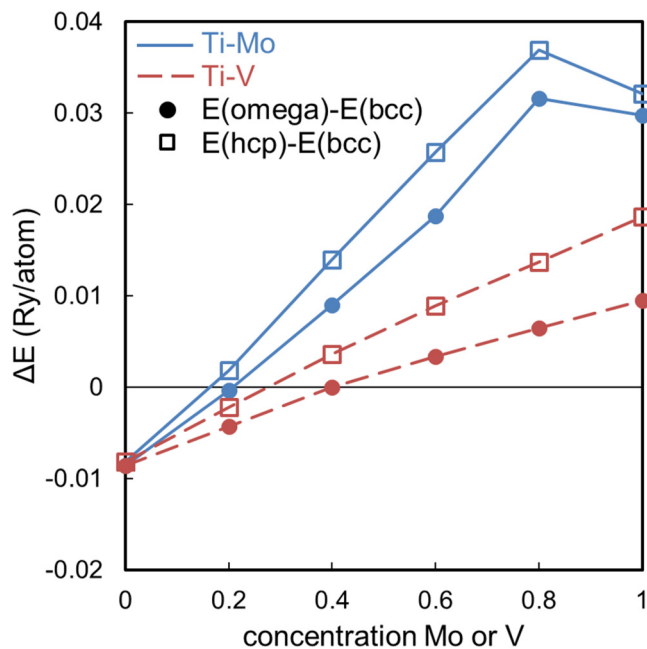


FIG. 1. Total energies differences of Ti-Mo and Ti-V alloys, QE-VCA.

The GB supercell contains 48 atoms. The right half ($x > 0$) consists of four blocks with the axes $x_0 = [111]/2$, $y_0 = [\bar{1}\bar{1}2]$, $z_0 = [1\bar{1}0]$ stacking along the x direction. The left half ($x < 0$) of the GB supercell is the right half mirrored with respect to the plane $x = 0$. The initial configuration is constructed using the calculated equilibrium bcc lattice parameter and ideal atomic positions. The x -dimension of the cell and internal atomic coordinates are subsequently relaxed, while the y and z dimensions remain unchanged. The result should resemble the coherent patch of a GB between misfit dislocations, though there is evidence that relaxing the y and z dimensions may slightly change the GB energetics [15,16]. The convergence criteria of atomic relaxation is when the total energy difference between two consecutive relaxation steps is smaller than 10^{-4} Ry and when all components of all forces are smaller than 10^{-3} Ry/Bohr (1 Bohr = 0.529177 Å).

B. Benchmarking VCA for Ti-Mo and Ti-V alloys

VCA is a single-site approximation where the pseudopotentials of pure elements are interpolated. The interpolation scheme for USPP described in the Appendix of Ref. [7] is adopted by QE. VCA is generally less accurate than Green's function-based formalisms of DFT using coherent potential approximation (CPA) [17–19] for chemical disorder. Therefore we have also used the exact muffin-tin orbital (EMTO) method [20,21] with CPA to calculate total energies, of which some details are explained in Appendix B.

For first-order transformations, the thermodynamic phase stabilities at 0 K is represented by total energy differences. The total energy differences of bcc, hcp, and ω Ti-Mo and Ti-V alloys are plotted in Fig. 1. Adding Mo or V to Ti lowers the bcc total energy with respect to the other two phases. The composition where two phases have the same total energy represents an equilibrium for composition-

invariant transformations and should be an extension of the composition-invariant equilibrium temperature to 0 K [22].

The equilibrium lattice parameters and second-order elastic constants of bcc Ti-Mo and Ti-V are calculated (Fig. 2). The experimental data of single-crystal elastic constants are scarce, but those of polycrystalline Young's modulus are abundant. Therefore, we convert C_{11} , C_{12} , and C_{44} to isotropic Young's modulus E by

$$64\mu^4 + 16(4C_{11} + 5C_{12})\mu^3 + [3(C_{11} + 2C_{12}) \times (5C_{11} + 4C_{12}) - 8(7C_{11} - 4C_{12})C_{44}]\mu^2 - (29C_{11} - 20C_{12})(C_{11} + 2C_{12})C_{44}\mu - 3(C_{11} + 2C_{12})^2(C_{11} - C_{12})C_{44} = 0, \quad (1)$$

$$B = (C_{11} + 2C_{12})/3, \quad (2)$$

$$E = 9B\mu/(3B + \mu), \quad (3)$$

where the equation for isotropic shear modulus μ is from Hershey [23] and B is bulk modulus.

The 0 K thermodynamic stability of bcc phase with respect to other phases, shown in Fig. 1, does not represent the mechanical stability of bcc on its own. In the harmonic approximation and under zero external load, a mechanically stable crystal must have real and positive phonon frequencies for all wave vectors and polarizations [29]. Otherwise, the crystal cannot sustain. The bcc structure can lose its mechanical stability by a soft shear modulus $C' = (C_{11} - C_{12})/2$ or a soft phonon mode Ω at wave vector $k_\Omega = (2/3)[111]$. The former is related to bcc-hcp transition and the latter to bcc- ω transition. Figure 3 summarizes the calculated C' modulus and Ω -phonon frequency ω_Ω . The bcc- ω stability can also be characterized by the energy change along its transition path, shown in Fig. 4. In bcc, the x coordinates of the (666) layers A, B, and C (Fig. 5) are 0, 1/3, and 2/3 times $x_0 = [111]/2$, respectively. Bcc transforms to (hexagonal) ω if layers B and C collapse into one layer at $1/2x_0$. The transition path can be described by a variable δ , with which the x coordinates of layers A, B, and C are 0, $1/3 + \delta/6$, $2/3 - \delta/6$. $\delta = 0$ stands for bcc and $\delta = 1$ for (hexagonal) ω . The energies shown in Fig. 4 are calculated from $\delta = 0$ to $\delta = 1$, with cell dimensions fixed to those of equilibrium bcc for simplicity.

QE-VCA calculations as in Figs. 3 and 4 suggest that about 20% Mo or 50% V is needed to make bcc structure mechanically stable. Experimentally, quenched-in ω particles cannot be detected by x-ray or neutron diffraction peaks beyond about 10% Mo [30] or 20% V [31], which coincide with the markings in Figs. 2(c) and 2(d). On the other hand, ω -like diffuse scattering can still be found in Ti-18% Mo [30] and Ti-40% V [32]. The critical concentrations found by QE-VCA seems more consistent with the disappearance of ω -like diffuse scattering, instead of the disappearance of quenched-in ω particles. However, the ω -like diffuse scattering is arguably brought about by chemical short-range order [33] and static atomic displacement [34], which VCA or any single-site approximation cannot account for.

Based the above comparisons between QE-VCA and EMTO-CPA or experimental data, we find VCA works satisfactorily well for the Ti-Mo and Ti-V systems as a

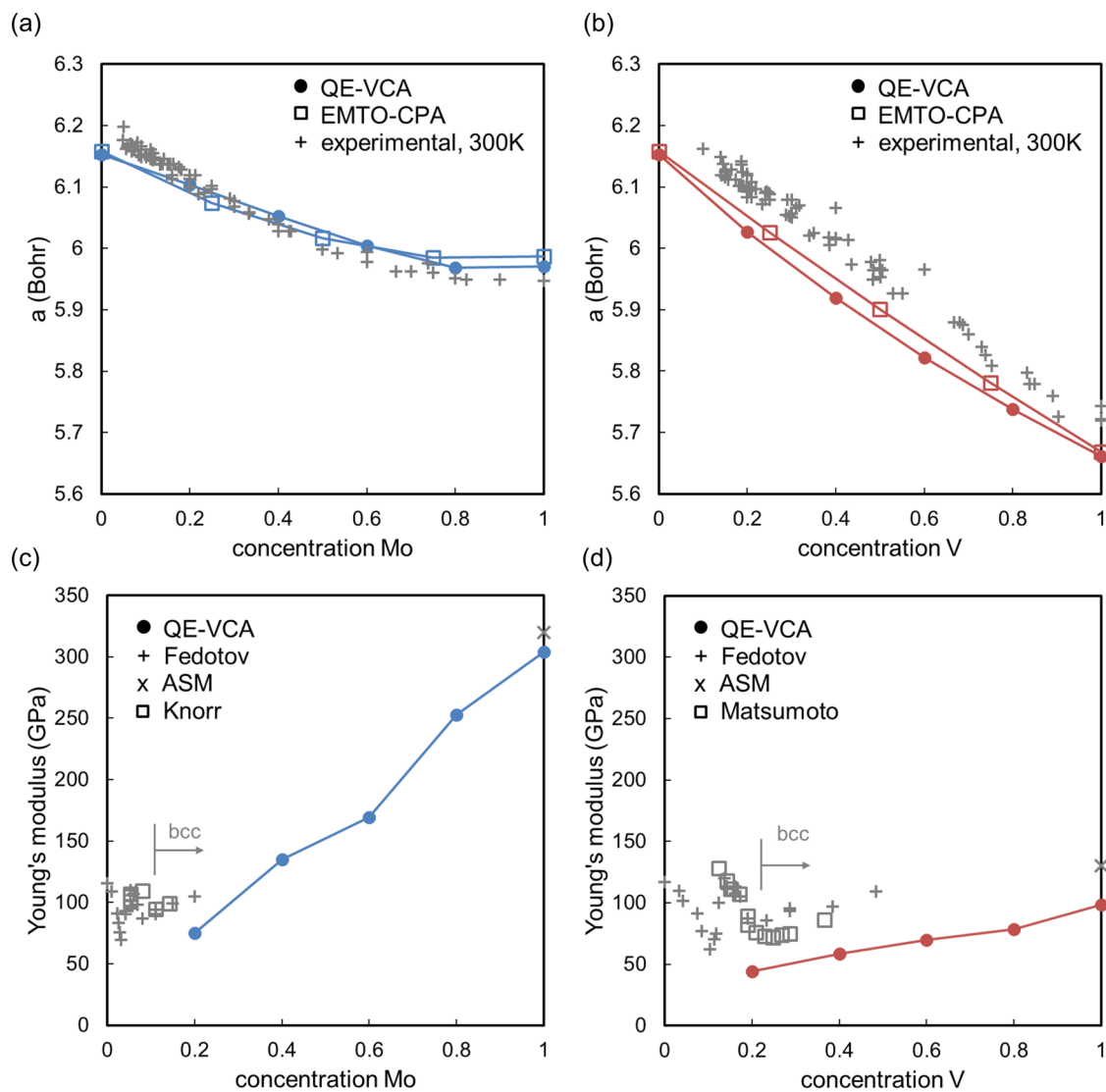


FIG. 2. Lattice parameter and polycrystalline Young's modulus of bcc Ti-Mo and Ti-V alloys. Experimental lattice parameters at 300 K are compiled in Ref. [24]. Experimental Young's modulus data at 300 K are from Refs. [25–28].

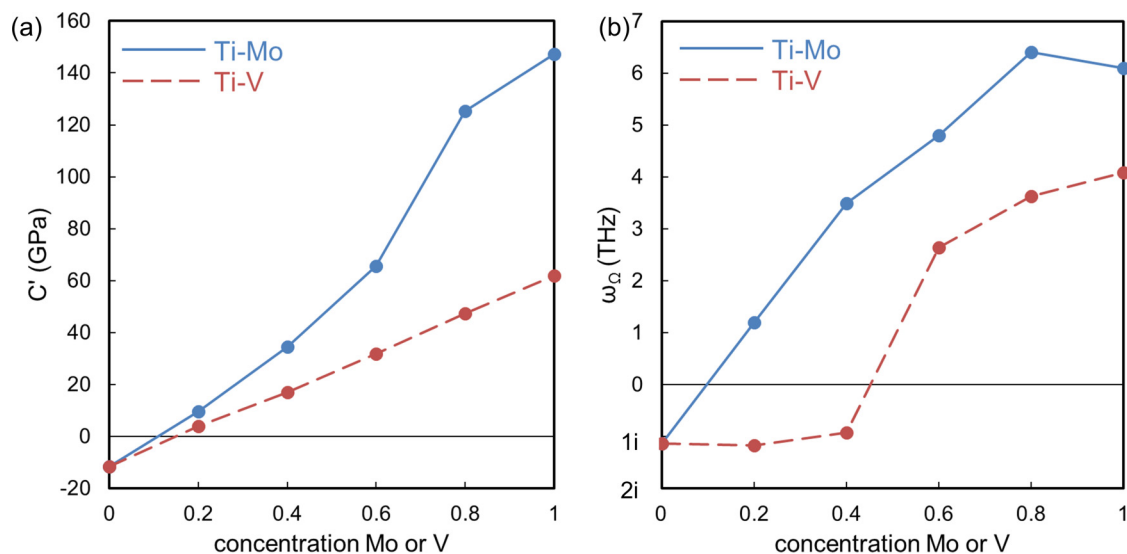


FIG. 3. C' shear modulus (a) and the phonon frequency (b) at wave vector $k_\Omega = (2/3)[111]$ of bcc Ti-Mo and Ti-V alloys, QE-VCA.

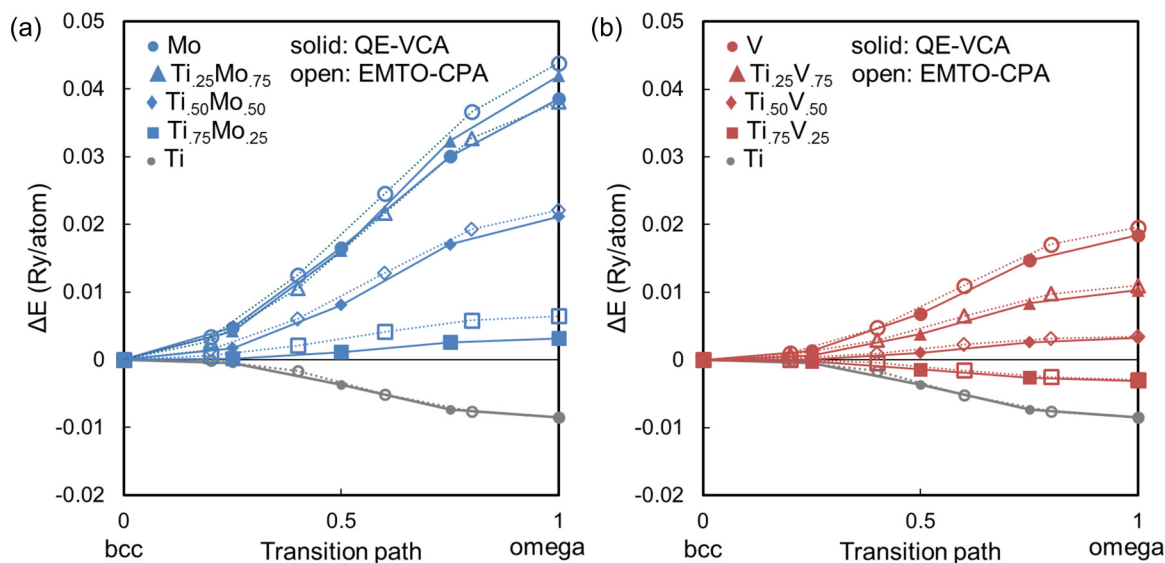


FIG. 4. Bcc- ω energy difference along the transition path (described in text) under constant volume.

single-site approximation. Discrepancies are largely contributed by pure elements rather than VCA as a mixing scheme. VCA cannot represent chemical short-range order or local atomic displacements, which become more important close to the mechanical instability of bcc. However, since our focus is the geometric configurations (atomic positions) near a GB, VCA saves the necessity of building “super-supercells” of the GB supercell for sampling chemical configurations (atomic species) as an extra level of complexity.

C. The GB supercell: Atomic configuration, valence electron density, and relaxation displacements

Figure 5 shows the valence electron density distribution in a bcc cell, suggesting the change of Ω -phonon frequency is directly related to a change in the total charge density

and its directional distribution. A stable bcc structure has higher electron density in $\langle 111 \rangle/2$ bonds than $\langle 100 \rangle$ bonds. As approaching the Ti side and the Ω -phonon instability, the total valence electron density is progressively lower, and the electron densities in $\langle 111 \rangle/2$ bonds and $\langle 100 \rangle$ bonds become closer. This motivates the atomic shuffle resulting in an ω structure, where the previous bcc $\langle 111 \rangle/2$ and $\langle 100 \rangle$ bonds become equivalent.

The cell in Fig. 5 is the building block of a $\Sigma 3[1\bar{1}0](111)$ GB supercell shown in Fig. 6. Upon relaxing the atomic coordinates in a GB supercell, Atoms ± 1 and ± 4 are displaced away from the GB (and so are Atoms ± 8 and ± 11 by inversion symmetry), while Atoms ± 2 and ± 5 (also Atoms ± 7 and ± 10) tend to fill the vacancy on the GB plane. Such displacements,

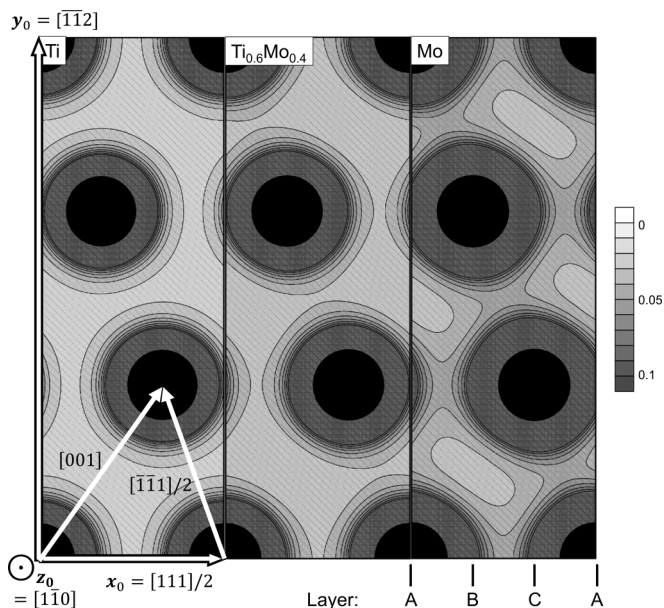


FIG. 5. Valence charge density in a bcc cell, QE-VCA.

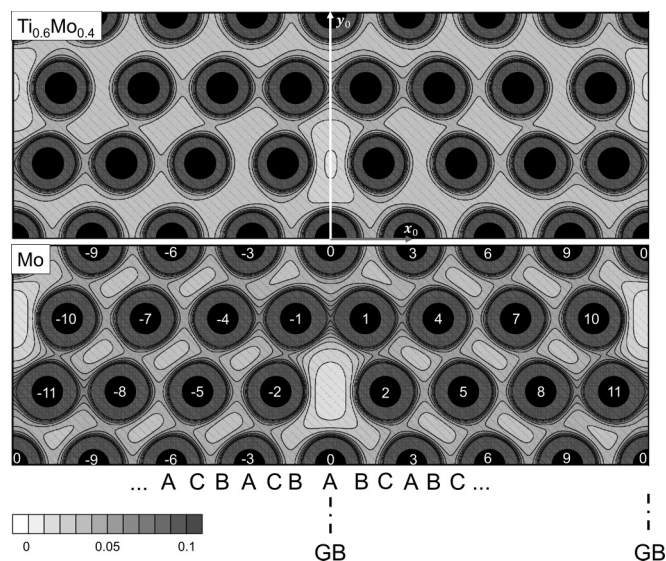


FIG. 6. Atomic positions and valence charge density of the relaxed GB supercells on the plane $z = 0$. The layer $z = z_0/2$ is the same but offset by $x_0/2$. The x dimension of the two supercells are not equal after relaxation but are scaled for clarity.

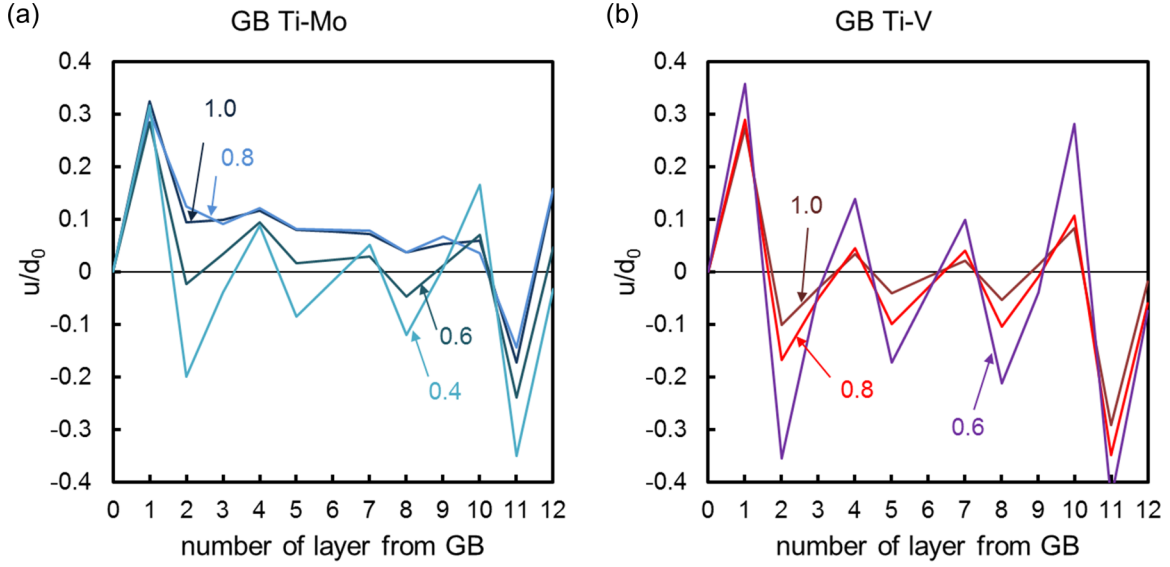


FIG. 7. Layer displacements u in bcc equilibrium interlayer spacing d_0 . Values pointing to the curves are atomic fractions of Mo or V. The displacement of layer 12 is V^{GB} because the x -dimension of the GB supercell is relaxed.

plotted in Fig. 7, results in a partially ω -like structure near the GB plane. The extent of the ω -like relaxation depends on the stiffness of bcc against ω -like distortion: a composition with higher bcc stability is more resistant to the disturbance near the GB and has a thinner layer of ω -like structure. It can also be described from an electronic density point of view: when the average electron density is low, the atoms favor a denser configuration and move toward the ω structure. When approaching the critical composition of bcc instability, the ω -like layer gets thicker to an extent that all atoms in the supercell are affected. Below the critical composition, the bcc GB structure will collapse to a fully ω phase structure after full relaxation.

D. GB energy, excess volume, and their correlations to bcc- ω phase stability

The GB energy E^{GB} and excess volume V^{GB} are listed in Table I. The V^{GB} is defined as the volume expansion per GB area, having a unit of length. To remove the effect of the composition dependence of lattice parameter, E^{GB} and V^{GB} are also expressed, respectively, in energy per atomic GB area and equilibrium interlayer spacing $d_0 = (\sqrt{6}/3)a_0$, where a_0 is the equilibrium bcc lattice parameter. Scheiber *et al.* [35] showed that a large number of GB structures of bcc Mo have

E^{GB} of $1.5 \sim 2.5 \text{ J/m}^2$ and V^{GB} of $0.2 \sim 0.6$ Bohr, while a few GBs have distinctly lower E^{GB} , about 0.6 J/m^2 , and almost zero V^{GB} . In terms of E^{GB} and V^{GB} , the majority group is termed “general” GB while the minority named “singular” GB [36]. The $\Sigma 3[1\bar{1}0](111)$ GB investigated in this work is a general GB, while the bcc twin boundary $\Sigma 3[1\bar{1}0](112)$ ($E^{\text{GB}} = 0.54 \text{ J/m}^2$ and $V^{\text{GB}} = -0.02$ Bohr for bcc Mo [35]) is singular.

Since the valence electron density and near GB displacements vary with bcc- ω phase stabilities, we plot the GB energy before and after relaxation, and the excess GB volume, against the bcc- ω phase stability (Fig. 8). The GB energies of Ti-Mo and Ti-V alloys before relaxation are two separate linear functions of bcc- ω energy difference, but after relaxation they fall into approximately one curve. The excess GB volume after relaxation of both series of alloys can be described very well by a linear function of bcc- ω energy difference. It is not clear though if such correlations apply to other elements or finite temperature.

III. MODEL CALCULATIONS

We now turn to an investigation of the GB structure and energetics using model pairwise interlayer interactions, which can be determined using smaller supercells. In metals, the interaction energies between ions screened by core electrons are pairwise, while the energy of valence electron distribution can be described as a functional of local density and density gradient [37]. Therefore, pairwise interlayer interaction as a model should work well provided the valence electron density distribution does not change much. The pairwise interlayer model we use for GB is essentially the same as the methods approximating stacking fault energy with structural energies [38].

The total GB energy is the sum of two components: the chemical component $E_{\text{chem}}^{\text{GB}}$, which is the GB energy with atoms on ideal bcc positions, and the relaxation component $E_{\text{rlx}}^{\text{GB}}$, which is the change in GB energy as a result of relaxation.

TABLE I. GB energy and excess volume.

	E^{GB} , Ry/atomic area	E^{GB} , J/m ²	V^{GB} , d_0	V^{GB} , Bohr
Mo	0.144	1.81	0.304	0.525
Ti _{0.2} Mo _{0.8}	0.194	2.45	0.317	0.546
Ti _{0.4} Mo _{0.6}	0.148	1.84	0.094	0.162
Ti _{0.6} Mo _{0.4}	0.095	1.17	-0.066	-0.115
V	0.094	1.32	-0.058	-0.094
Ti _{0.2} V _{0.8}	0.073	1.00	-0.080	-0.132
Ti _{0.4} V _{0.6}	0.051	0.68	-0.149	-0.251

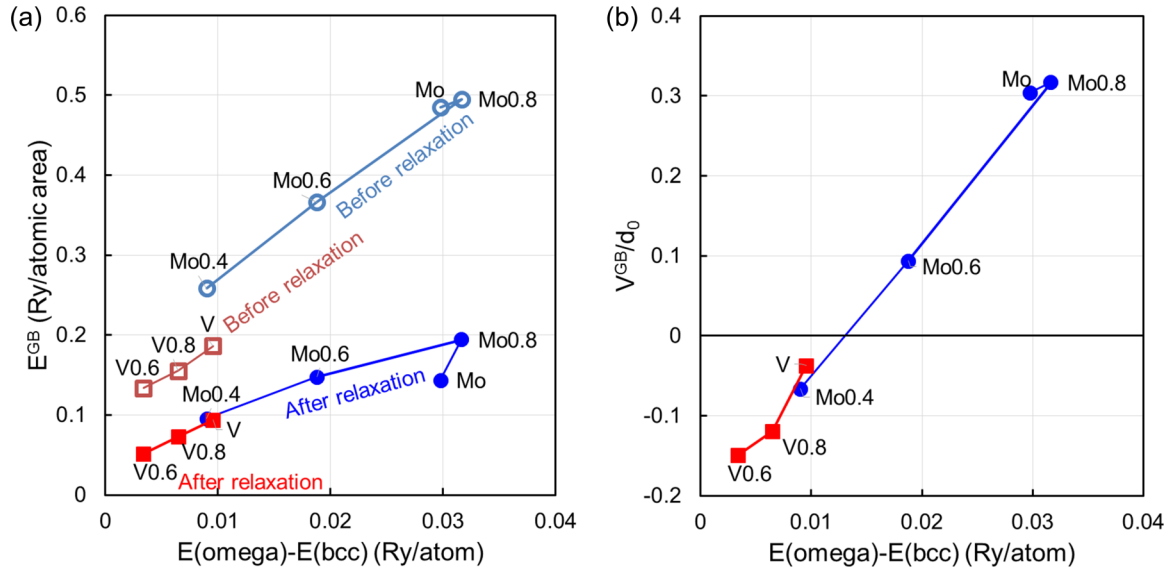


FIG. 8. The correlations of (a) GB energy E^{GB} before and after relaxation and (b) excess GB volume V^{GB} to bcc- ω phase stability.

A. Interlayer interactions and the chemical component of GB energy

The stacking sequence of bcc (666) planes can be expressed by ... ABC ... with a period of 3 (Fig. 5). The equilibrium interlayer spacing $d_0 = |(1/6)[111]_{\text{bcc}}| = (\sqrt{3}/6)a_0$, where a_0 is the equilibrium bcc lattice parameter. Due to symmetry, the interlayer interactions are grouped into (1) interactions of like layers: $\phi_{aa} \equiv \phi_{AA} = \phi_{BB} = \phi_{CC}$; and (2) interactions of unlike layers: $\phi_{ab} \equiv \phi_{AB} = \phi_{BC} = \phi_{CA} = \phi_{AC} = \phi_{CB} = \phi_{BA}$. In the ABC sequence (bcc), the energy per layer is

$$\begin{aligned} E_0 &= \phi_{ab}(d_0) + \phi_{ab}(2d_0) + \phi_{aa}(3d_0) + \phi_{ab}(4d_0) \\ &\quad + \phi_{ab}(5d_0) + \phi_{aa}(6d_0) + \dots \\ &= \sum_{k=1}^{+\infty} \phi_{ab}[(3k-2)d_0] + \phi_{ab}[(3k-1)d_0] + \phi_{aa}[3kd_0]. \end{aligned} \quad (4)$$

However, near a GB the stacking sequence is disturbed (Fig. 6). We define the excess interaction due to a ‘‘wrong’’ pair compared to ABC:

$$\Delta_n \equiv \begin{cases} \phi_{ab}(nd_0) - \phi_{aa}(nd_0), & \text{if } n = 3k \\ \phi_{aa}(nd_0) - \phi_{ab}(nd_0), & \text{if } n = 3k - 2 \text{ or } 3k - 1 \end{cases} \quad (5)$$

By analyzing the change in pair correlation near a GB, the excess energy upon introducing a GB is

$$\begin{aligned} E_{\text{chem}}^{\text{GB}} &= (\Delta_2 + 2\Delta_3 + \Delta_4) + 2(\Delta_5 + 2\Delta_6 + \Delta_7) \\ &\quad + 3(\Delta_8 + 2\Delta_9 + \Delta_{10}) + \dots \\ &= \sum_{k=1}^{+\infty} k(\Delta_{3k-1} + 2\Delta_{3k} + \Delta_{3k+1}), \end{aligned} \quad (6)$$

which can be named the ‘‘chemical’’ component GB energy, because it does not involve relaxation and is determined by atomic species.

We find the Δ_n terms by considering some other stacking sequences:

- ... AB ... (period 2),
- ... ABAC ... (period 4),
- ... ABCAB ... (period 5),
- ...

By comparing pair correlations to the ABC structure, the energy difference between a structure S per period and bcc can be written as a sum of Δ_n terms:

$$\Delta_S \equiv E_S - N_S E_0 = \sum_n p_S(n) \Delta_n, \quad (7)$$

where N_S is the number of layers per period of structure S . The coefficients $p_S(n)$ are listed in Table II.

To find N terms $\Delta_2, \dots, \Delta_{N+1}$ we need N structures whose coefficient vectors $\{s(2), \dots, s(N+1)\}$ are linearly independent. An example of linear dependency is the structure ABCACB, because $\Delta_{\text{ABCACB}} = -\Delta_{\text{AB}} + \Delta_{\text{ABABAC}}$. The N terms $\Delta_2, \dots, \Delta_{N+1}$ form the solution of a set of linear equations. For example, if $N = 5$, we use all the five linearly independent structures listed in Table II, then

$$\begin{bmatrix} 2 & 2 & 2 & 0 & 0 \\ 2 & 4 & 4 & 0 & 2 \\ 2 & 3 & 0 & 5 & 5 \\ 4 & 6 & 4 & 0 & 0 \\ 2 & 4 & 3 & 2 & 7 \end{bmatrix} \begin{bmatrix} \Delta_2 \\ \Delta_3 \\ \Delta_4 \\ \Delta_5 \\ \Delta_6 \end{bmatrix} = \begin{bmatrix} \Delta_{\text{AB}} \\ \Delta_{\text{ABC}} \\ \Delta_{\text{ABCAB}} \\ \Delta_{\text{ABABAC}} \\ \Delta_{\text{ABCACB}} \end{bmatrix} \quad (8)$$

Combining Table II and Eq. (6) for $E_{\text{chem}}^{\text{GB}}$, we can also find by Gaussian elimination a series of expansions to an arbitrary accuracy in principle:

$$\begin{aligned} E_{\text{chem}}^{\text{GB}} &= 0.5\Delta_{\text{ABAC}} - \Delta_4 + 2\Delta_5 + 3\Delta_6 + \dots \\ E_{\text{chem}}^{\text{GB}} &= -0.5\Delta_{\text{AB}} + 0.5\Delta_{\text{ABABAC}} \\ &\quad + 2\Delta_5 + 4\Delta_6 + 2\Delta_7 + \dots \end{aligned}$$

TABLE II. Coefficients $p_S(n)$.

$n \setminus S$	AB	ABAC	ABCAB	ABABAC	ABCACBC
1	0	0	0	0	0
2	2	2	2	4	2
3	2	4	3	6	4
4	2	4	0	4	3
5	0	0	5	0	2
6	0	2	5	0	7
7	$p(n+6)$ $= p(n)$	0	2	$p(n+6)$ $= p(n)$	7
8		4	2		0
9		4	5		5
10		2	5		3
11		0	0		3
12		0	3		5
13		$p(n+12)$ $= p(n)$	2		0
14			0		7
15			0		7
16			$p(n+15)$ $= p(n)$		2
17					3
18					4
19					2
20					0
21					0
...					$p(n+21)$ $= p(n)$

$$E_{\text{chem}}^{\text{GB}} = -0.1\Delta_{\text{AB}} + 0.4\Delta_{\text{ABAC}} + 0.4\Delta_{\text{ABCAB}} - 0.1\Delta_{\text{ABABAC}} + 1.2\Delta_6 + 1.2\Delta_7 + 1.2\Delta_8 + \dots$$

$$E_{\text{chem}}^{\text{GB}} = -\frac{1}{16}\Delta_{\text{AB}} + \frac{1}{16}\Delta_{\text{ABAC}} + \frac{1}{4}\Delta_{\text{ABCAB}} - \frac{1}{16}\Delta_{\text{ABABAC}} + \frac{3}{8}\Delta_{\text{ABCACBC}} - 1\frac{1}{8}\Delta_7 + 2\frac{5}{8}\Delta_8 + 3\frac{1}{8}\Delta_9 + \dots \quad (9)$$

With reference to the direct supercell calculations with 12 layers between two GBs (Sec. II C), the expansion Eq. (9) converges quite well (Fig. 9). For alloys with a lower bcc stability, the convergence is slower, but in principle any accuracy can be obtained provided a sufficient number of linearly independent stacking sequences.

B. Relaxation and excess GB volume

Figure 7 shows that near GB there are significant displacements of atomic layers from their ideal bcc positions. In this section we attempt to solve the relaxation of the atomic layers near the GB.

In Sec. III A we have identified the mismatched layers near the GB and their energies. The fact there exists relaxation implies that there is also “residual forces” between the mismatched layers if they stay on their ideal bcc positions. We Taylor expand Δ_n with respect to the displacement u from the ideal distance nd_0 :

$$\Delta_n(u) = \Delta_n + \Delta'_n u + \frac{1}{2}\Delta''_n u^2 + \left(\frac{1}{6}\Delta'''_n u^3 + \frac{1}{24}\Delta''''_n u^4\right), \quad (10)$$

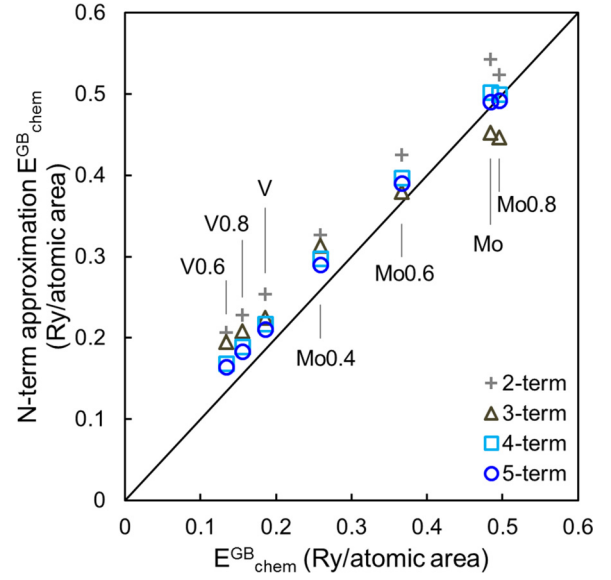


FIG. 9. Chemical GB energy approximated using a number of stacking sequences.

where

$$\Delta'_n \equiv \begin{cases} \frac{d(\phi_{ab}-\phi_{aa})}{dx} \Big|_{x=nd_0}, & n = 3k \\ \frac{d(\phi_{aa}-\phi_{ab})}{dx} \Big|_{x=nd_0}, & n = 3k - 2 \text{ or } 3k - 1 \end{cases}$$

and higher-order derivatives $\Delta''_n, \Delta'''_n, \Delta''''_n$ are defined similarly. $\Delta'_n = -f_n$ is the negative residual force ($\Delta'_n > 0$ for tension; < 0 for compression) and Δ''_n is the excess force constant between two mismatched layers nd_0 apart. We repeat the calculations of Eq. (8) with varied interlayer spacing and fit Eq. (10) to the $\Delta_n(u)$ terms. We expand $\Delta_3(u), \Delta_4(u), \dots$ up to the second order but $\Delta_2(u)$ to the fourth order, because of the large displacements of layers $(N-1)$ and (1) due to a strong repulsion. Figure 10 shows the expansions for Mo.

Far from the GB, the structure restores the undisturbed bcc (666) planes, and the displacements can be solved based on

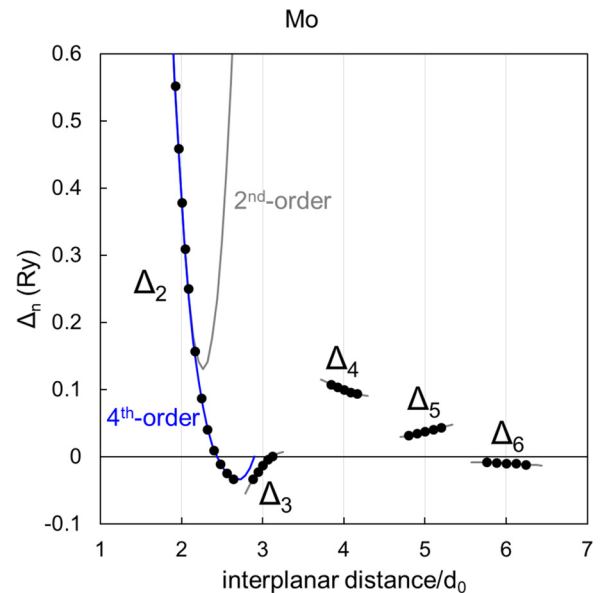


FIG. 10. Δ_n and Taylor expansions about nd_0 for Mo. Second-order expansion for all in gray and fourth-order in blue for Δ_2 only.

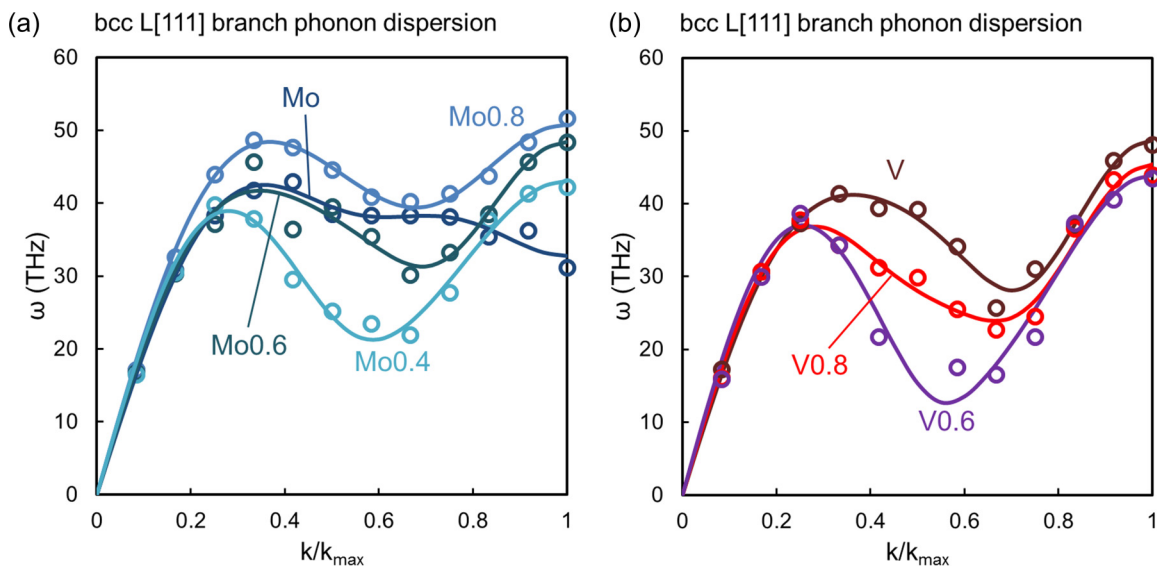


FIG. 11. bcc L[111] phonon frequencies calculated by density-functional perturbation theory (open circles) and their Fourier transforms (solid lines) with the coefficients in Table IV.

TABLE III. Δ_n and their derivatives.

Ry	Δ_2	Δ_3	Δ_4	Δ_5	Δ_6
Mo	0.3784	-0.0125	0.0994	0.0379	-0.0096
Ti _{0.2} Mo _{0.8}	0.3570	0.0034	0.0826	0.0346	-0.0058
Ti _{0.4} Mo _{0.6}	0.2990	0.0145	0.0511	0.0160	-0.0052
Ti _{0.6} Mo _{0.4}	0.2380	0.0276	0.0197	0.0010	-0.0063
V	0.1554	0.0169	0.0350	0.0046	-0.0057
Ti _{0.2} V _{0.8}	0.1453	0.0195	0.0241	-0.0031	-0.0048
Ti _{0.4} V _{0.6}	0.1448	0.0175	0.0152	-0.0084	-0.0035
Ry/Bohr	Δ'_2	Δ'_3	Δ'_4	Δ'_5	Δ'_6
Mo	-1.0919	0.0830	-0.0245	0.0173	-0.0035
Ti _{0.2} Mo _{0.8}	-0.9989	0.0802	-0.0190	0.0251	-0.0086
Ti _{0.4} Mo _{0.6}	-0.8063	0.1004	-0.0469	0.0072	-0.0024
Ti _{0.6} Mo _{0.4}	-0.5661	0.0820	-0.0520	-0.0068	0.0040
V	-0.4763	0.0877	-0.0502	0.0067	-0.0016
Ti _{0.2} V _{0.8}	-0.4053	0.0731	-0.0475	0.0023	0.0002
Ti _{0.4} V _{0.6}	-0.3613	0.0699	-0.0455	-0.0018	0.0017
Ry/Bohr ²	Δ''_2	Δ''_3	Δ''_4	Δ''_5	Δ''_6
Mo	2.3993	-0.1708	0.0309	0.0003	-0.0039
Ti _{0.2} Mo _{0.8}	1.9193	-0.0195	-0.0184	-0.0091	-0.0047
Ti _{0.4} Mo _{0.6}	1.5729	-0.1170	0.0376	0.0253	-0.0073
Ti _{0.6} Mo _{0.4}	1.2981	-0.1237	0.0378	0.0201	-0.0050
V	1.0515	-0.1531	0.0855	0.0341	-0.0069
Ti _{0.2} V _{0.8}	1.0875	-0.1439	0.0527	0.0168	0.0007
Ti _{0.4} V _{0.6}	0.9940	-0.0969	0.0318	0.0109	-0.0016
Ry/Bohr ³	Δ'''_2	Ry/Bohr ⁴	Δ'''_2		
Mo	-4.097	Mo	4.053		
Ti _{0.2} Mo _{0.8}	-2.293	Ti _{0.2} Mo _{0.8}	0.9697		
Ti _{0.4} Mo _{0.6}	-2.066	Ti _{0.4} Mo _{0.6}	1.27		
Ti _{0.6} Mo _{0.4}	-2.877	Ti _{0.6} Mo _{0.4}	3.942		
V	-1.466	V	0.7697		
Ti _{0.2} V _{0.8}	-2.763	Ti _{0.2} V _{0.8}	4.195		
Ti _{0.4} V _{0.6}	-2.743	Ti _{0.4} V _{0.6}	4.394		

TABLE IV. Interlayer force constants of bcc (111) planes by Fourier transforming the L[111] phonon dispersion, Ry/Bohr².

	γ_1	γ_2	γ_3	γ_4	γ_5
Mo	0.0503	0.1046	0.0595	0.0443	–
Ti _{0.2} Mo _{0.8}	0.1025	0.0668	0.1255	0.0120	0.0096
Ti _{0.4} Mo _{0.6}	0.0699	0.0226	0.1045	–0.0015	0.0175
Ti _{0.6} Mo _{0.4}	0.0351	–0.0235	0.0850	0.0292	0.0126
V	0.0427	0.0137	0.0740	–0.0088	0.0123
Ti _{0.2} V _{0.8}	0.0320	–0.0132	0.0625	0.0060	0.0161
Ti _{0.4} V _{0.6}	0.0243	–0.0387	0.0628	0.0218	0.0153

the knowledge of phonon dispersion along longitudinal [111] branch of the equilibrium bcc structure. The interlayer force constants $\{\gamma_p\}$ can be obtained by Fourier transforming the phonon dispersion [39,40]:

$$m\omega^2(k) = \sum_{p=1}^N \gamma_p \left(1 - \cos \frac{p\pi k}{k_{\max}} \right). \quad (11)$$

For the ABC stacking sequence, $\gamma_1 = \phi''_{ab}|_{d_0}$, $\gamma_2 = \phi''_{ab}|_{2d_0}$, $\gamma_3 = \phi''_{aa}|_{3d_0}$, $\gamma_4 = \phi''_{ab}|_{4d_0}$, ..., and $k_{\max} = (2\pi/a_0)\sqrt{3} = \pi/d_0$. In practice the Fourier series is truncated to N terms if γ_{N+1} and above is negligible and the obtained $\{\gamma_p\}$ do not change much with increasing N . We find $N = 4$ acceptable for Mo and 5 for the other cases. The force constants are listed in Table IV, and Fig. 11 plots the phonon dispersions from direct calculations and using Eq. (11) with Table IV. We notice a significant decrease in γ_1 and γ_2 as the composition approaches Ti.

Given the excess bond energy, residual forces, excess force constants due to layer mismatch from Table III and the bcc force constants from Table IV, we are ready to tackle the GB relaxation problem.

The interlayer problem with GB is equivalent to the problem of a one-dimensional chain of N_p oscillators, but with an impurity (the GB) which changes the bond energy and stiffness and brings about residual forces within a number of nearest neighbors. We assume the Born–von Kármán periodic boundary condition but allow the period of the chain to change. The energy caused by relaxation is

$$E_{\text{rlx}}^{\text{GB}} = \sum_{i=1}^{N_p} \sum_{s=1}^{N_g} \left[\delta_{is} \Delta_i^{(s)} \left(\sum_{p=1}^s b_{i+p-1} \right) + \frac{1}{2} (\gamma_i^{(s)} + \delta_{is} \Delta_i^{(s)}) \left(\sum_{p=1}^s b_{i+p-1} \right)^2 \right] + \frac{1}{6} \Delta_{N_p-1}^{(2)} (b_{N_p-1} + b_{N_p})^3 + \frac{1}{24} \Delta_{N_p-1}^{(4)} (b_{N_p-1} + b_{N_p})^4. \quad (12)$$

We define u_i as the displacement of layer i , and b_i as $u_{i+1} - u_i$, i.e., the change in the distance between layers $(i+1)$ and i . The distance between layers $(i+s)$ and i is then $\sum_{p=1}^s b_{i+p-1}$. From here on all the subscripts for u and b are modulo N_p , for example, $u_{N_p+1} = u_1$, $u_{-1} = u_{N_p-1}$. The δ_{is} marks whether there is a mismatch: $\delta_{is} = 1$ if the layers i and

$i+s$ are mismatched compared to the bcc stacking sequence, and 0 otherwise. Up to the sixth neighbor, the mismatched layers near the GB are:

s (index of nearest neighbor)	i for $\delta_{is} = 1$ in Eq. (12)
2	$N_p - 1$
3	$N_p - 2, N_p - 1$
4	$N_p - 2$
5	$N_p - 4, N_p - 1$
6	$N_p - 5, N_p - 4, N_p - 2, N_p - 1$
...	...

among which only the interaction between layers $(N_p - 1)$ and (1) are treated up to the fourth order.

We minimize $E_{\text{rlx}}^{\text{GB}}$ with respect to $\{b_i\}_{i=1}^{N_p}$. If the cubic and quartic terms are neglected, the minimization can be done by matrix algebra. With cubic or higher-order terms, it is convenient to minimize $E_{\text{rlx}}^{\text{GB}}$ numerically. The minimization can be done with the constraint $\sum_{i=1}^{N_p} b_i = 0$, which means the total length of the chain does not change, or without the constraint in which case the change in the period is given by $\sum_{i=1}^{N_p} b_i = u_{N_p} = V^{\text{GB}}$.

We calculated the equilibrium relaxation GB energy (Fig. 12), normalized excess GB volume V^{GB}/d_0 (Fig. 13),

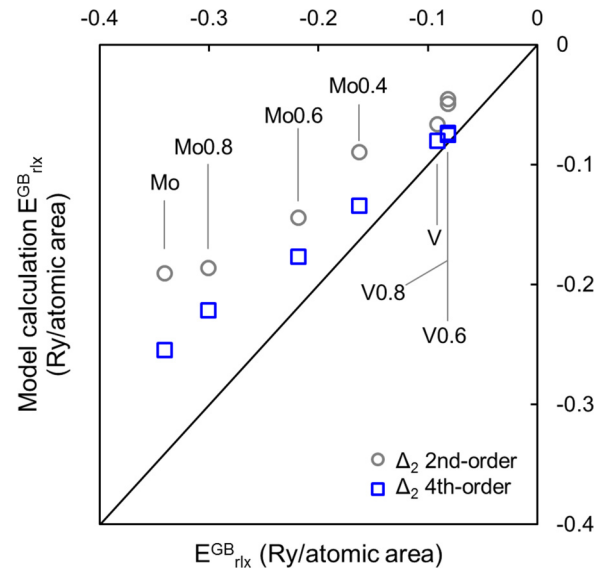


FIG. 12. Relaxation GB energy, model calculations versus ab initio results. Gray dots correspond to second-order expansion of Δ_2 and blue dots correspond to fourth-order approximation of Δ_2 .

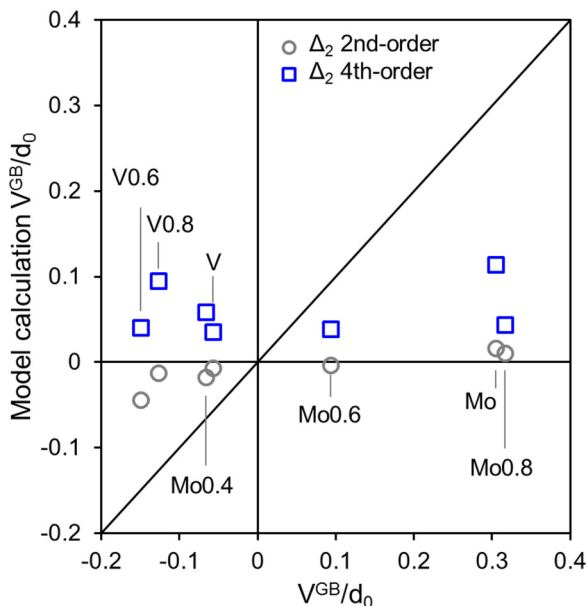


FIG. 13. Excess GB volume, model calculations versus *ab initio* results. Gray circles correspond to second-order expansion of Δ_2 and blue squares correspond to fourth-order approximation of Δ_2 .

and equilibrium displacements (Fig. 14) using parabolic or quartic approximation of Δ_2 . Obviously, the parabolic approximation of Δ_2 yields too-high energy and stiffness when the distance between layers ($N_p - 1$) and (1) are large, therefore significantly underestimates the relaxation displacements. The local harmonic approximation accounts for about 60% of the relaxation energy. Using a quartic fitting to Δ_2 (while keeping the zeroth to the second derivatives) improves the prediction of relaxation displacements and is able to account for about 70% of the relaxation energy, but still much underestimates the near-GB displacements.

It is expected that the relaxation can be better modeled if more anharmonic terms are added, for example, the third-order force constants in bcc. The necessity of anharmonic

pairwise terms or even going beyond pairwise approximation is especially obvious regarding the excess GB volume, which is not well reproduced using the current model calculations.

Surprisingly, the excess GB volume from direct supercell calculations is well correlated to the total energy difference between ω and bcc [Fig. 8(b)]. Recall that the stacking sequence of ω is the same as bcc except that every two of three layers merge. Therefore, the correlation between excess GB volume and $E(\omega) - E(\text{bcc})$ may imply that the higher-order force constants in the ABC stacking sequence plays a more important role than the excess interactions between mismatched layers. It is not clear yet whether $E(\omega) - E(\text{bcc})$ is a good indicator for V^{GB} for other chemistry or even at finite temperature.

Another source of discrepancy lies in the method of calculating Δ_n and their derivatives: we stretched various stacking sequences uniformly, which implies a uniform average interstitial electronic density. This may not be applicable to the region near GB, where the gradient of electronic density is strong. However, to account for the aforementioned factors, much more calculations are required, and the advantage of calculating small cells may be lost.

C. Harmonic vibration near the equilibrium positions

After equilibrium positions are found, now we consider harmonic vibrations about the equilibrium positions. Writing the time-dependent part of displacement as $u(t) = u_i^d \exp(i\omega t)$, the vibrational displacement follows

$$-m_i \omega^2 u_i^d = \sum_s [(\gamma_i^{(s)} + \delta_{is} \Delta_i^{(s)''}) (u_{i+s}^d - u_i^d) - (\gamma_{i-s}^{(s)} + \delta_{is} \Delta_{i-s}^{(s)''}) (u_i^d - u_{i-s}^d)], \quad (13)$$

which is an eigenproblem:

$$D u^d = \omega^2 u^d, \quad (14)$$

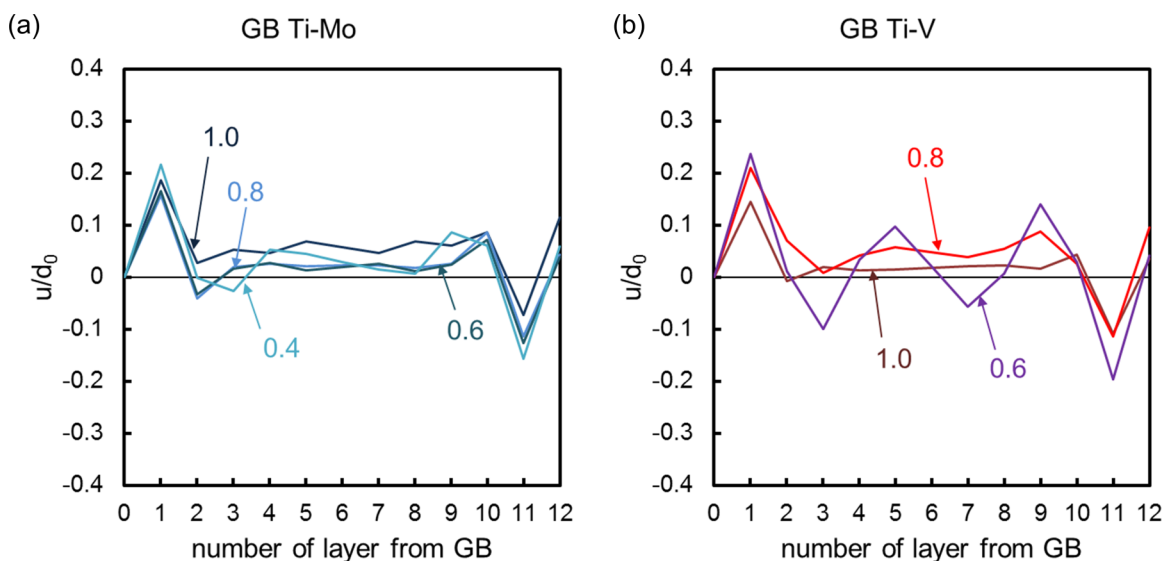


FIG. 14. Atomic displacements from model calculations, Δ_2 quartic.

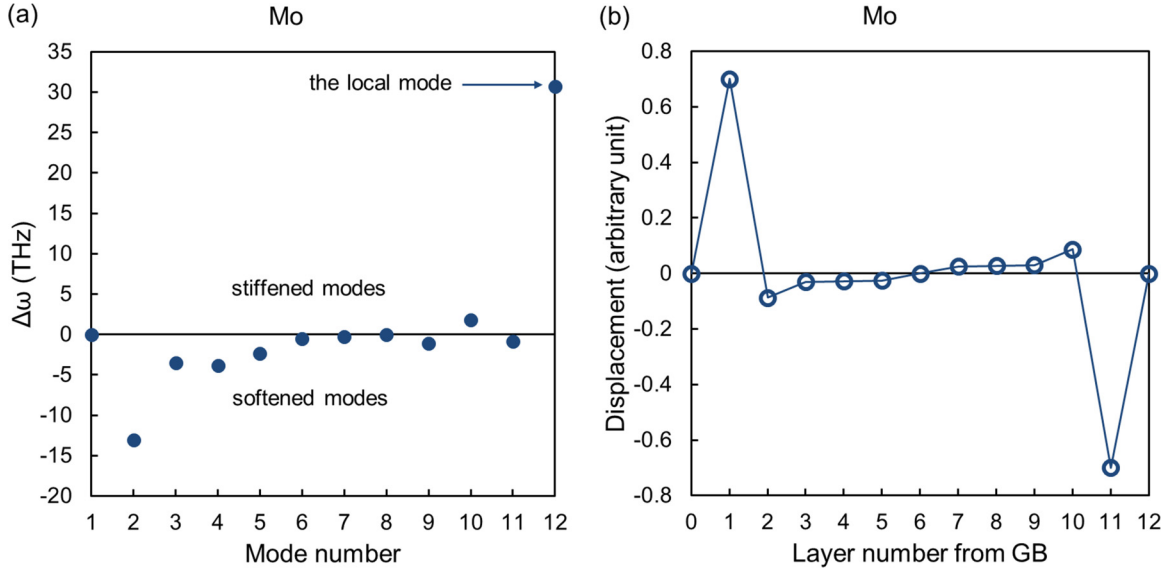


FIG. 15. (a) Difference in the eigenstate frequencies between the supercell with GB and the supercell without GB (pure bcc) of Mo. Both have 12 layers per period. There are some modes softened ($\Delta\omega < 0$), also a strongly stiffened oscillator, the local mode. (b) The eigenvector, i.e., the vibrational displacement pattern, associated with the local mode, which is obviously not a plane wave.

with the N_p eigenvalues being the vibrational frequencies squared ω_λ^2 and their corresponding eigenvectors being the displacement pattern in real space, $u_{i,\lambda}^d$.

In harmonic approximation, the force constants are independent of atomic displacements. However, this is not the case if a higher-order Taylor expression is used for Δ_2 . In the following, we present the results using the Δ_2'' at the ideal position (local harmonic approximation), to the results using the Δ_2'' at the equilibrium position.

Compared to the pure ABC stacking sequence, the eigenvalues of an impurity chain includes a local mode [Fig. 15(a)], which means it is an isolated eigenstate out of the spectrum of frequencies of a pure ABC sequence. This is because some bonds near the GB are much stiffened. There are also softened bonds near the GB which give rise to frequency shifts to the lower side. Many eigenvectors for the impurity chain are not lattice waves which has a unique wave vector, but wave packets with a spectrum of wave vectors, for example, the eigenvector corresponding to the local mode [Fig. 15(b)].

If we take every eigenstate as a phonon, even if it is not a plane wave in real space, we can write out the vibrational free energy of the system,

$$F_{\text{vib}}(T) = \sum_{\lambda} \left\{ \frac{\hbar\omega_{\lambda}}{2} + k_B T \log \left[1 - \exp \left(-\frac{\hbar\omega_{\lambda}}{k_B T} \right) \right] \right\}. \quad (15)$$

The excess vibrational free energy of the GB per atomic area is the difference between the free energy of a chain with GB and that of a purely bcc chain, which is shown in Fig. 16. Comparing the two calculations using $\Delta_2''(2d_0)$ and $\Delta_2''(2d_0 + 2u_1^{\text{eq}})$, the former stiffness is much higher, giving rise to a much higher local phonon mode and a negative excess vibrational entropy, which may be physically unrealistic. In contrast, the excess vibrational free energy using the latter stiffness decreases with increasing temperature, which is expected for most kinds of defects. We need to emphasize that (1) the $\Delta F_{\text{vib}}(T)$ calculated here assumes the GB only

disturbs the L[111] phonon branch of bcc but not the other branches, and (2) the volume dependence of force constants, which may have a negative contribution to $\Delta F_{\text{vib}}(T)$, is not considered.

IV. DISCUSSION

A. Relaxation displacements within bcc

The pattern of the relaxation displacements within bcc depends on the phonon properties solely, which can be found by the following method based on Ref. [41].

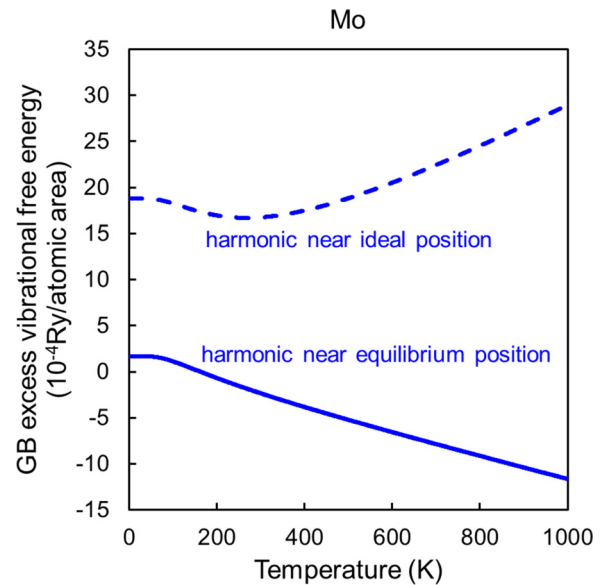


FIG. 16. GB excess vibrational free energy of Mo using harmonic approximation near ideal position, $\Delta_2''(2d_0)$, and near equilibrium position, $\Delta_2''(2d_0 + 2u_1^{\text{eq}})$ for the interaction between layers $(N-1)$ and (1).

Suppose the force constants are known by invoking Eq. (11). Using trigonometric equations, $\cos p\theta$ can be always expressed as an p th-order polynomial of $\cos \theta$. Therefore, Eq. (11) can be rewritten as

$$m\omega^2(k) = \sum_{p=0}^N a_p \cos^p(\pi k/k_{\max}), \quad (16)$$

where the coefficients a_p are functions of the force constants γ_s . For example, if $N = 5$, then $a_0 = \gamma_1 + 2\gamma_2 + \gamma_3 + \gamma_5$, $a_1 = -\gamma_1 + 3\gamma_3 - 5\gamma_5$, $a_2 = -2\gamma_2 + 8\gamma_4$, $a_3 = -4\gamma_3 + 20\gamma_5$, $a_4 = -8\gamma_4$, and $a_5 = -16\gamma_5$. Relaxation implies a static solution, i.e., $\omega = 0$, and the problem is finding the N roots of the N th-order polynomial on the right-hand side of Eq. (16), which are

$$k = 0, \{k_R + ik_I\}_{N-1}, \quad (17)$$

where k_R and k_I are real. The only real root is 0, because there is no zero or imaginary phonon frequency on the dispersion curve except the origin. The other roots are complex. A static lattice wave with the complex wave vector $k = k_R + ik_I$ is

$$u(x) = c \exp(ikx) = c \exp(-k_I x) \exp(ik_R x), \quad (18)$$

which is a lattice wave with wave vector k_R (or a period of $2\pi/k_R$) with an exponentially decaying or growing amplitude $u_0 \exp(-k_I x)$. The general displacement is a linear combination of the waves in Eq. (18) plus a linear term for $k = 0$:

$$u(x) = c_0 + c_1 x + \sum_{r=2}^N c_r \exp(-k_I^{(r)} x) \exp(ik_R^{(r)} x). \quad (19)$$

The coefficients are to be determined by boundary conditions. Given $u(x)$, it is also possible to obtain the relaxation GB energy within bcc analytically.

However, we do not carry out such calculations in this work because (1) it does not account for all the relaxation GB energy, and (2) we have four or five force constants, making the analysis quite complicated without gaining much physical significance.

B. Effect of finite GB spacing

Usually two GBs with an inversion center are put in a supercell, and the convergence with respect to GB spacing is examined. This is more convenient to carry out using pairwise interlayer interactions compared to direct supercell calculations.

For the chemical GB energy, if we examine the pair correlations between finite and infinite GB spacing, it is easy to find out the leading truncation error due to a finite GB spacing (Table V). The DFT results using different GB spacing values are shown in Fig. 17. Compared to Fig. 9, we can see

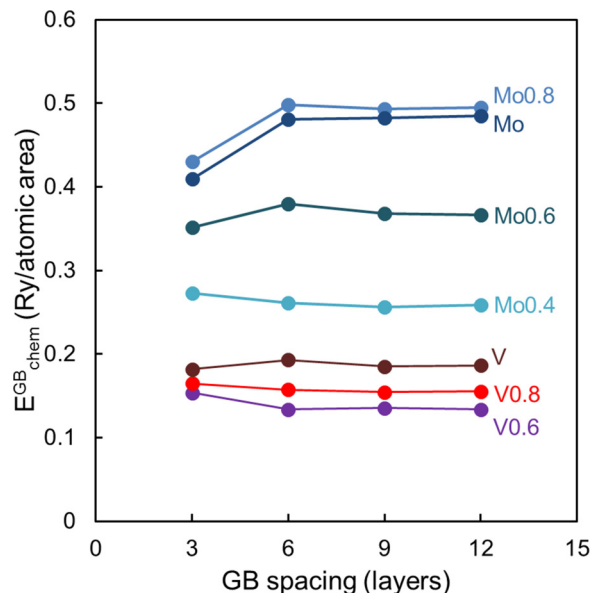


FIG. 17. Convergence of the chemical part of GB energy with respect to GB spacing (DFT results).

the $E_{\text{chem}}^{\text{GB}}$ from $N_p = 3$ is comparable to $E_{\text{chem}}^{\text{GB}}$ approximated using Eq. (9), because the leading truncation errors of both approximations are on the order of Δ_5 . The computational cost of the method in Sec. III A may be comparable or even larger to that of directly enlarging GB spacing. However, a great advantage of the former method is the ability of separating Δ_n terms and getting their derivatives.

For the relaxation, we find the relaxation energy and excess GB volume by numerical minimization. The results for Mo and $\text{Ti}_{0.4}\text{V}_{0.6}$, representing the two extremes of bcc stability, are presented in Fig. 18. From the model calculations we can see using a supercell with GB spacing equal to 12 layers is already good enough, where the truncation error is less than the discrepancy between model calculations and first-principles results. The GB vibrational free energy also converges with increasing supercell size.

V. CONCLUSIONS

(1) Virtual crystal approximation (VCA) works reasonably well for Ti-Mo and Ti-V alloys as a single-site approximation. Calculated 0 K thermodynamic phase stabilities, bcc lattice parameters, and elastic constants are well compared to experimental data and EMTO-CPA calculations. It can reflect the bcc-stabilizing effect of Mo and V on Ti. Using VCA, a series of alloys can be generated with various bcc stabilities. When

TABLE V. Leading truncation error in the chemical component of GB energy using supercells.

Stacking sequence	GB spacing, number of layers (N_p)	Leading truncation error in $E_{\text{chem}}^{\text{GB}}$
... ABCACB ... (period 6)	3	$2\Delta_5 + 4\Delta_6 + 2\Delta_7 + \dots$
... ABCABCACBACB ... (period 12)	6	$2\Delta_8 + 4\Delta_9 + 2\Delta_{10} + \dots$
(period 18)	9	$2\Delta_{11} + 4\Delta_{12} + 2\Delta_{13} + \dots$
(period 24)	12	$2\Delta_{14} + 4\Delta_{15} + 2\Delta_{16} + \dots$
...

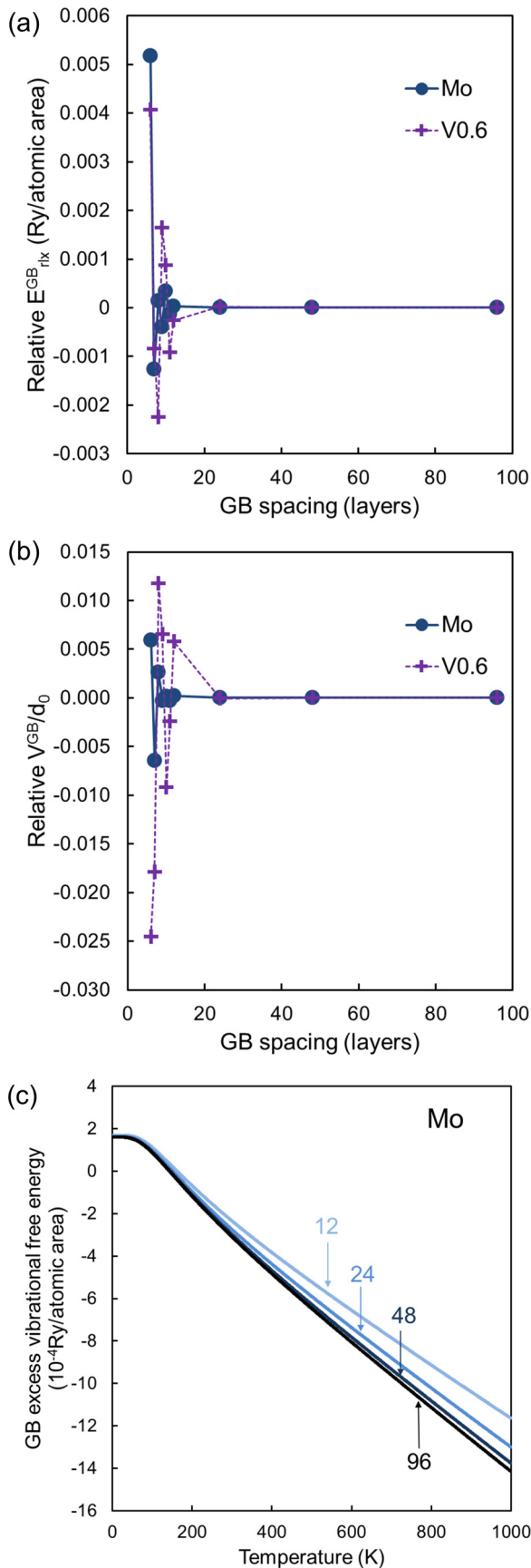


FIG. 18. Convergence of (a) relaxation GB energy, (b) excess GB volume, and (c) GB excess vibrational free energy with respect to GB spacing, by model calculations.

bcc instability is approached, there is a depletion of average interstitial valence electron density, and the electron density in $(1/2)[111]$ bcc bonds and that in $[100]$ bcc bonds tend to be similar.

(2) The energetics and atomic structures of $\Sigma 3[1\bar{1}0](111)$ GB of bcc Ti-Mo and Ti-V alloys are obtained using first-principles total energy calculations of supercells at 0 K. The GB creates an ω -like atomic shuffle whose magnitude decays with increasing distance from GB. Approaching bcc instability, the GB relaxation extends increasingly deeper into the bulk. After relaxation, the GB energy and the excess GB volume correlate with bcc- ω phase stability.

(3) The energy of any stacking sequences of bcc (666) planes can be analyzed using pairwise interlayer interactions. The chemical GB energy can be expressed as a sum of excess interlayer interactions caused by a mismatch with reference to the bcc stacking sequence. The excess interactions can be solved to an arbitrary number of terms using the total energies of periodic structures with various stacking sequences. The chemical GB energy converges well with increasing number of periodic structures considered to the results from supercell calculations.

(4) The energy associated with the relaxation near the GB is solved by numerical minimization using the derivatives of the excess interactions with respect to interplanar distance. It is necessary to include anharmonic contributions for the interactions of layers, which undergo large relaxation displacements. Current models can account for about 70% of the relaxation energy of GB. The excess GB volume is sensitive to the method approximating interlayer potentials. Higher-order force constants of bcc and effects of nonhomogeneous electron density are possibly responsible for the discrepancies.

(5) The phonon spectrum of a supercell with a GB has a local mode whose frequency is higher than the maximal frequency of a pure bcc crystal, caused by the stiffened interlayer interactions near the GB. There are also softened interactions, which give rise to a shift of vibrational frequency to the lower side. The excess vibrational free energy of the GB is calculated under harmonic approximation. Using the force constants near the equilibrium positions, rather than the ideal positions, gives a negative temperature dependence of the excess GB vibrational free energy, as expected.

ACKNOWLEDGMENTS

The computations were performed on resources provided by the Swedish National Infrastructure for Computing (SNIC) at NSC, Linköping University (SNIC 2015/1-403), and PDC, KTH Royal Institute of Technology (PDC-2016-67), Sweden. The authors also appreciate the constructive comments from the anonymous reviewers, and Dr. Daniel Scheiber (Material Center Leoben, Austria) for sending raw data from Ref. [35].

APPENDIX A: SEGREGATION ENERGIES OF B AND Y TO A SUBSTITUTIONAL SITE ON THE GB

For the GB segregation energies of B and Y, the energies of GB cells with the host atom “O” substituted by the segregant. Also needed is the energies of B or Y in a bcc supercell without GB. This is carried out using a bcc supercell of the same size as

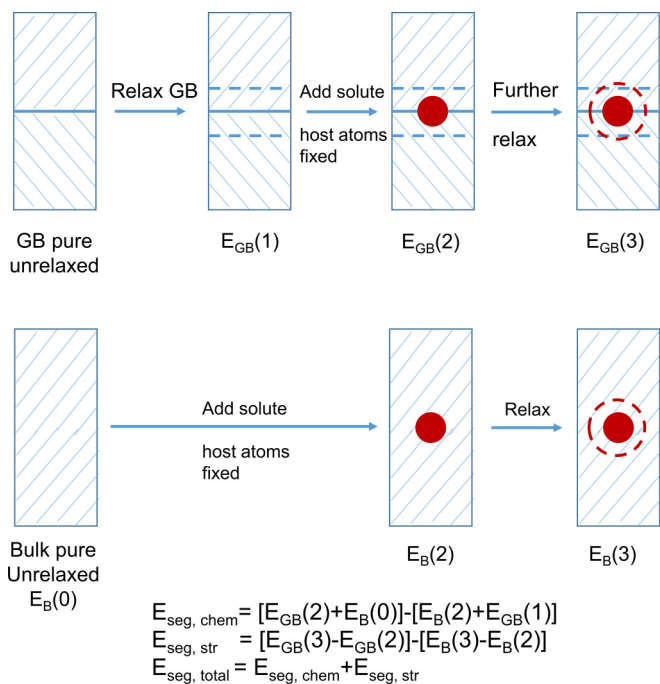


FIG. 19. Energies related to GB segregation and the definition of segregation energy and its chemical and strain-induced components.

the GB supercell, in order to avoid to the largest extent artifacts due to different solute concentration and image interactions.

The relevant energetics is summarized in Fig. 19. E_{seg} is the energy difference between the final and start states of segregation. Negative E_{seg} means segregation is favored, while positive E_{seg} implies antisegregation. E_{seg} can be divided into a chemical component and a strain-induced one.

The segregation energies for B and Y in four of the GBs are listed in Table VI. The results show that Y tends to segregate to the substitutional site on GB, while B tends to antisegregate to the site.

The reliability of GB-segregation energy has been examined in relation to the solubility of the segregant in the host crystal by Lejček *et al.* [42,43]. Their conclusion is the calculated segregation energy is reliable if the solute concentration in the supercell is smaller than its solubility in the host bulk. Otherwise, the supercell calculation represents a nonequilibrium state and the so-obtained segregation energy cannot be used in equilibrium calculations. The solute concentration in the supercell is $1/48 \approx 2.1\%$. The maximum solubilities of B in bcc Ti, Mo, and V are about 1% [44], 0.8% [45], and 1 ~ 2% [46], respectively, while those of Y in bcc Ti, Mo, and V are about 1% [47], 0.1% [48], and

TABLE VI. Segregation energies of B and Y to the bcc $\Sigma 3[1\bar{1}0](111)$ GBs of Ti-Mo and Ti-V (negative = segregation).

E_{seg} , eV	B			Y		
	Chemical	Strain	Total	Chemical	Strain	Total
Ti _{0.6} Mo _{0.4}	0.14	0.01	0.15	-0.36	<-0.16	<-0.51
Mo	0.86	-0.22	0.63	-0.02	-0.07	-0.08
Ti _{0.4} V _{0.6}	0.02	0.10	0.12	0.05	-0.06	-0.01
V	0.10	-0.17	-0.06	-0.32	-0.25	-0.57

~ 0 [49], respectively. Therefore it requires further investigations to determine whether the calculated segregation energies of B and Y can be used for equilibrium calculations.

Our calculations do not exclude the possibility of B segregating to an interstitial site. In addition, the results with the alloyed host atoms can be viewed as preliminary, because (1) near the bcc instability of the host, the segregant atom causes excessive relaxation near the GB, and (2) VCA does not account for local chemical correlations.

APPENDIX B: DETAILS OF EMTO CALCULATIONS

For the EMTO calculations in this work, we adopt the full charge density (FCD) formalism [13,20,21], where we first calculate the electronic structure using the local density approximation by Perdew and Wang [50], then use such electron density to calculate the total energy using the GGA by Perdew, Burke, and Ernzerhof [10]. All the self-consistent EMTO-CPA calculations are performed using an orbital momentum cutoff $l_{\text{max}} = 3$ for partial waves.

The onsite screening contribution to the electrostatic potential v_{scr}^i of alloying element i , and the energy E_{scr}^i of a random alloy are included in the electronic structure and total-energy calculations in order to account for the effects of charge transfer between alloying elements, within the single-site approximation [51–54]:

$$v_{\text{scr}}^i = -e^2 \alpha_{\text{scr}}^i \frac{q_i}{S}, \quad (\text{B1})$$

$$E_{\text{scr}}^i = \frac{1}{2} \beta_{\text{scr}}^i \sum_i c_i q_i v_{\text{scr}}^i, \quad (\text{B2})$$

where c_i is the concentration of element i , and q_i is the net charge in the atomic sphere of element i , S is the Wigner–Seitz radius, α_{scr}^i and β_{scr}^i are two parameters. In this work, α_{scr}^i and β_{scr}^i in single-site EMTO-CPA calculations are determined from the locally self-consistent Green’s function method [55–57] calculations for 384-atom disordered supercells. The screening parameter β_{scr}^i is a fitting parameter about unity which simply renormalizes the electrostatic energy of single-site CPA to that of the corresponding supercell. β_{scr}^i is not exactly unity due to the multipole–multipole interactions in the supercell where local symmetry is reduced. However, calibration calculations show that the deviation of β_{scr}^i from unity has a negligible effect on the total energies calculated in this work. Therefore, we set β_{scr}^i to 1 for all the cases in this work. α_{scr}^i is calculated by

$$\alpha_{\text{scr}}^i = -\frac{S(\langle v_i \rangle - \bar{v})}{e^2 \langle q_i \rangle}, \quad (\text{B3})$$

where $\langle q_i \rangle$ and $\langle v_i \rangle$ are the q_i and v_i averaged over the supercell, and $\bar{v} = \sum_i c_i \langle v_i \rangle$ is the total average Madelung potential. \bar{v} has a small nonzero value even in highly symmetric cubic crystal due to multipole moments of the electron density. For binary alloys, the α_{scr}^i parameters of the two elements are equal [58].

The calculated α_{scr} of Ti-Mo and Ti-V alloys depend on alloy composition and crystal structure. In bcc Ti-Mo, α_{scr} ranges from 0.81 to 1.0. In ω Ti-Mo, the α_{scr} of site 1 (with 14 nearest neighbors) varies from 0.77 to 1.0, while that of sites 2

and 3 (equivalent, both with 11 nearest neighbors) varies from 0.97 to 1.0. The α_{scr} of bcc Ti-V ranges from 0.50 to 0.56. In ω Ti-V, the difference in α_{scr} between inequivalent sites is small. It is expected that Ti-Mo exhibits a larger magnitude and a

stronger composition dependence of α_{scr} than Ti-V, because Mo contributes more d electrons than V.

The screening parameters along the bcc- ω transformation path are determined by linear interpolation.

-
- [1] S. Banerjee and P. Mukhopadhyay, *Phase Transformations: Examples from Titanium and Zirconium Alloys* (Elsevier, New York, 2010).
- [2] Z.-G. Mei, S.-L. Shang, Y. Wang, and Z.-K. Liu, *Phys. Rev. B* **80**, 104116 (2009).
- [3] O. Hellman, I. A. Abrikosov, and S. I. Simak, *Phys. Rev. B* **84**, 180301 (2011).
- [4] O. Hellman, P. Steneteg, I. A. Abrikosov, and S. I. Simak, *Phys. Rev. B* **87**, 104111 (2013).
- [5] A. I. Duff, T. Davey, D. Korbmayer, A. Glensk, B. Grabowski, J. Neugebauer, and M. W. Finnis, *Phys. Rev. B* **91**, 214311 (2015).
- [6] S. Kadkhodaei, Q.-J. Hong, and A. van de Walle, *Phys. Rev. B* **95**, 064101 (2017).
- [7] L. Bellaiche and D. Vanderbilt, *Phys. Rev. B* **61**, 7877 (2000).
- [8] P. Giannozzi *et al.*, *J. Phys.: Condens. Matter* **21**, 395502 (2009).
- [9] K. F. Garrity, J. W. Bennett, K. M. Rabe, and D. Vanderbilt, *Comput. Mater. Sci.* **81**, 446 (2014).
- [10] J. P. Perdew, K. Burke, and M. Ernzerhof, *Phys. Rev. Lett.* **77**, 3865 (1996).
- [11] M. Methfessel and A. T. Paxton, *Phys. Rev. B* **40**, 3616 (1989).
- [12] H. J. Monkhorst and J. D. Pack, *Phys. Rev. B* **13**, 5188 (1976).
- [13] L. Vitos, *Computational Quantum Mechanics for Materials Engineers: The EMTO Method and Applications* (Springer, London, 2007).
- [14] S. Baroni, S. de Gironcoli, A. Dal Corso, and P. Giannozzi, *Rev. Mod. Phys.* **73**, 515 (2001).
- [15] T. Ochs, C. Elsässer, M. Mrovec, V. Vitek, J. Belak, and J. A. Moriarty, *Philos. Mag. A* **80**, 2405 (2000).
- [16] T. Ochs, O. Beck, C. Elsässer, and B. Meyer, *Philos. Mag. A* **80**, 351 (2000).
- [17] P. Soven, *Phys. Rev.* **156**, 809 (1967).
- [18] B. L. Györfy, *Phys. Rev. B* **5**, 2382 (1972).
- [19] J. S. Faulkner, *Prog. Mater. Sci.* **27**, 1 (1982).
- [20] L. Vitos, *Phys. Rev. B* **64**, 014107 (2001).
- [21] L. Vitos, I. A. Abrikosov, and B. Johansson, *Phys. Rev. Lett.* **87**, 156401 (2001).
- [22] J.-Y. Yan and G. B. Olson, *J. Alloys Compd.* **673**, 441 (2016).
- [23] A. V. Hershey, *J. Appl. Mech.* **21**, 236 (1954).
- [24] J.-Y. Yan and G. B. Olson, *Calphad* **52**, 152 (2016).
- [25] S. G. Fedotov, in *Titanium Science and Technology*, edited by R. I. Jaffee and H. M. Burte (Plenum Press, New York, 1973), p. 871.
- [26] W. Knorr and H. Scholl, *Z. Metallk.* **51**, 605 (1960).
- [27] H. Matsumoto, S. Watanabe, N. Masahashi, and S. Hanada, *Metall. Mater. Trans. A* **37**, 3239 (2006).
- [28] *ASM Handbook Volume 2: Properties and Selection: Nonferrous Alloys and Special-Purpose Materials* (ASM International, Materials Park, Ohio, 1990).
- [29] G. Grimvall, B. Magyari-Kope, V. Ozolins, and K. A. Persson, *Rev. Mod. Phys.* **84**, 945 (2012).
- [30] C. Leibovitch, E. Gartstein, and A. G. Rabinkin, *Z. Metallk.* **71**, 438 (1980).
- [31] G. Aurelio, A. F. Guillermet, G. J. Cuello, and J. Campo, *Metall. Mater. Trans. A* **33**, 1307 (2002).
- [32] N. B. Dyakonova, I. V. Lyasotsky, and G. I. Nosova, *Rev. Adv. Mater. Sci.* **18**, 703 (2008).
- [33] W. Sinkler and D. E. Luzzi, *Acta Metall. Mater.* **42**, 1249 (1994).
- [34] I. B. Ramsteiner, O. Shchyglo, M. Mezger, A. Udyansky, V. Bugaev, S. Schoder, H. Reichert, and H. Dosch, *Acta Mater.* **56**, 1298 (2008).
- [35] D. Scheiber, R. Pippin, P. Puschnig, and L. Romaner, *Modell. Simul. Mater. Sci. Eng.* **24**, 035013 (2016).
- [36] A. P. Sutton and R. W. Balluffi, *Interfaces in Crystalline Materials* (Clarendon Press, London, 1995).
- [37] M. Finnis, *Interatomic Forces in Condensed Matter* (Oxford University Press, Oxford, 2003).
- [38] R. Li, S. Lu, D. Kim, S. Schönecker, J. Zhao, S. K. Kwon, and L. Vitos, *J. Phys.: Condens. Matter* **28**, 395001 (2016).
- [39] A. J. E. Foreman and W. M. Lomer, *Proc. Phys. Soc., London, Sect. B* **70**, 1143 (1957).
- [40] B. N. Brockhouse, T. Arase, G. Caglioti, K. R. Rao, and A. D. B. Woods, *Phys. Rev.* **128**, 1099 (1962).
- [41] B. Houchmandzadeh, J. Lajzerowicz, and E. Salje, *J. Phys.: Condens. Matter* **4**, 9779 (1992).
- [42] P. Lejčák, M. Šob, V. Paidar, and V. Vitek, *Scr. Mater.* **68**, 547 (2013).
- [43] P. Lejčák, M. Šob, and V. Paidar, *Prog. Mater. Sci.* **87**, 83 (2017).
- [44] J. L. Murray, P. K. Liao, and K. E. Spear, *Bull. Alloy Phase Diagrams* **7**, 550 (1986).
- [45] K. E. Spear and P. K. Liao, *Bull. Alloy Phase Diagrams* **9**, 457 (1988).
- [46] K. E. Spear, P. K. Liao, and J. F. Smith, *J. Phase Equilib.* **8**, 447 (1987).
- [47] W.-p. Gong, T.-f. Chen, D.-j. Li, and Y. Liu, *Trans. Nonferrous Met. Soc. China* **19**, 199 (2009).
- [48] W. Chan, M. C. Gao, Ö. N. Doğan, and P. King, *J. Phase Equilib. Diffus.* **31**, 414 (2010).
- [49] W. Chan, M. C. Gao, Ö. N. Doğan, and P. King, *J. Phase Equilib. Diffus.* **31**, 425 (2010).
- [50] J. P. Perdew and Y. Wang, *Phys. Rev. B* **45**, 13244 (1992).
- [51] I. A. Abrikosov, Y. H. Vekilov, P. A. Korzhavyi, A. V. Ruban, and L. E. Shilkrot, *Solid State Commun.* **83**, 867 (1992).
- [52] P. A. Korzhavyi, A. V. Ruban, I. A. Abrikosov, and H. L. Skriver, *Phys. Rev. B* **51**, 5773 (1995).
- [53] A. V. Ruban and H. L. Skriver, *Phys. Rev. B* **66**, 024201 (2002).
- [54] A. V. Ruban, S. I. Simak, P. A. Korzhavyi, and H. L. Skriver, *Phys. Rev. B* **66**, 024202 (2002).
- [55] I. A. Abrikosov, A. M. N. Niklasson, S. I. Simak, B. Johansson, A. V. Ruban, and H. L. Skriver, *Phys. Rev. Lett.* **76**, 4203 (1996).
- [56] I. A. Abrikosov, S. I. Simak, B. Johansson, A. V. Ruban, and H. L. Skriver, *Phys. Rev. B* **56**, 9319 (1997).
- [57] O. E. Peil, A. V. Ruban, and B. Johansson, *Phys. Rev. B* **85**, 165140 (2012).
- [58] P. A. Korzhavyi, A. V. Ruban, J. Odqvist, J. O. Nilsson, and B. Johansson, *Phys. Rev. B* **79**, 054202 (2009).